Vol 18 No 7, July 2009
1674-1056/2009/18(07)/2928-05

Chinese Physics B

© 2009 Chin. Phys. Soc.
and IOP Publishing Ltd

Phonon spectra of $La_{0.5}Ca_{0.5}MnO_3$*

Cao Xian-Sheng(曹先胜) and Chen Chang-Le(陈长乐)†

Shaanxi Key Laboratory of Condensed Matter Structures and Properties, School of Science, Northwestern Polytechnical University, Xi'an 710072, China

(Received 30 July 2008; revised manuscript received 25 December 2008)

This paper presents a microscopic theory to explain different Raman modes of $La_{0.5}Ca_{0.5}MnO_3$ based on the electronic Hamiltonian of the Kondo lattice model, which adds phonon interaction to the hybridization between the conduction electrons of the system and the l-electrons. The spectral density is calculated by the Green function technique of Zubarev at zero wave vector and in the low temperature limit. It finds that there are three Raman-active modes and the spectral densities of these modes are substantially influenced by model parameters such as the position of l-level ($\varepsilon_{\rm JT}$), the effective electron–phonon coupling strength (g) and the hybridization parameter (v). Finally, the intensity changes of those peaks are investigated.

Keywords: perovskite, Raman spectra
PACC: 7000, 6320K

1. Introduction

The perovskite-like manganites $R_{1-x}A_xMnO_3$, are characterized by a strong interplay of magnetism, electric transport and crystallographic distortion where R is a trivalent rare earth or Y, and A is a divalent alkaline earth element. At doping levels $0.15 < x < 0.45$ these materials exhibit colossal magnetoresistance near the concomitant ferromagnetic and insulator–metal transitions. At a fractional doping level, such as $x = 0.5$, the crystallographic and magnetic environment is strongly modified and charge ordering between Mn^{3+} and Mn^{4+} or phase separation takes place.[1−6]

Raman spectroscopy is a sensitive tool for the study of both local and spatially coherent structural changes. The formation of a superstructure usually results in the appearance of additional lines in the Raman spectra due to folding of the Brillouin zone and a decrease of the site symmetry for some atoms. Therefore, it is plausible to expect that changes of the Raman spectra in the charge- and orbital-ordered (COO) phase could provide valuable information about the structure and lattice dynamics of the COO state.[7−9] Thus, this technique affords a means by which energy and symmetry information regarding phonons, electrons, and spin excitations can be simultaneously explored. The first-order Raman phonon spectrum of a nominally perfect crystal consists of a series of narrow lines, which correspond to Raman-allowed zone-centre (Γ-point) phonon modes and obey definite polarization selection rules.[9,10] Therefore, we can use Raman spectroscopy to study the lattice distortions of $La_{0.5}Ca_{0.5}MnO_3$. In addition, no theoretical work has been done on Raman spectra of perovskite with a composition of 0.5.

In the present work, we use Raman active phonons to study the normal state behaviour of the doped system. For this purpose we describe the electronic Hamiltonian of the Kondo lattice model and introduce an electron–phonon interaction in Section 2. The phonon Green function is calculated in Section 3. The phonon spectral density is reported in Section 4. The results and discussion are given in Section 5.

2. Model

We start from the pictorial characteristic of systems with Jahn–Teller (JT) ions having an interplay between electrons localized due to lattice distortions and those in the band states. This situation is typical for manganites and can be described in terms of the Kondo-lattice model in the double-exchange limit taking account of the JT distortions and the super-exchange interaction between the localized electrons.[11] The intra-atomic exchange coupling is assumed to be large enough to align the spins of $e_{\rm g}$ electrons in a Mn ion parallel to the spin S of the core ($t_{2\rm g}$) electrons. The Jahn–Teller effect leads to a split-

*Project supported by the National Natural Science Foundation of China (Grant No 60171034).
†E-mail: chenchl@nwpu.edu.cn

ting of the double-degenerate e_g level. Then, following Ref.[12], we can divide e_g electrons into two groups: 'localized' (l, $t^{(l)} \to 0$) electrons which produce the maximum splitting of the e_g level and itinerant 'band' (b) electrons with non-zero hopping integrals t leading to smaller distortions of the MnO_6 octahedra. For simplicity of calculation, t does not change with θ_{ij} (the angle between local spin S_i and S_j), so the corresponding effective Hamiltonian has the form[11]

$$H_{\text{eff}} = -t\sum_{\langle ij\rangle}\left(c_i^+ c_j + \text{h.c.}\right) - \varepsilon_{\text{JT}}\sum_i n_{li} + J\sum_{\langle ij\rangle}\cos\theta_{ij} + U\sum_i n_{li}n_{bi}, \quad (1)$$

where ε_{JT} is the JT energy gain for l electrons counting from the center of the b-electron band, J is the exchange interaction energy and U is the Coulomb repulsion energy. Equation (1) describes the intra-atomic Hubbard interaction between the l-electrons and $l-b$-electrons, where $n_{li} = l_i^+ l_i$ and $n_{bi} = c_i^+ c_i$. We linearize the on-site l-electron interaction terms $l_i^+ l_i$ and $c_i^+ c_i$ in the Hamiltonian in the Hartree–Fock approximation as $n_{li}n_{bi} \to \langle n_{li}\rangle n_{bi} + n_{li}\langle n_{bi}\rangle$, where $\langle n_{li}\rangle = \langle l_i^+ l_i\rangle$ and $\langle n_{bi}\rangle = \langle c_i^+ c_i\rangle$ are the expectation values of n_{li} and n_{bi} respectively, and we take $\langle n_{li}\rangle = n_l$, $\langle n_{bi}\rangle = n_b$ for all i. The number of localized electrons n_{li}, and band electrons n_{bi} per lattice site obey an obvious relation $n_b + n_l = 1 - x$ (x is doping concentration, its value is 0.5). Then Hamiltonian H_{eff} reduces to

$$H_{\text{eff}} = -t\sum_{\langle ij\rangle} c_i^+ c_j - \varepsilon_{\text{JT}}\sum_i n_{li} + J\sum_{\langle ij\rangle}\cos\theta_{ij} + U\left(\sum_i n_{li}c_i^+ c_i + \sum_i l_i^+ l_i n_{bi}\right), \quad (2)$$

where $n_{bi} = c_i^+ c_i$; $n_{li} = l_i^+ l_i$ $\varepsilon_{\text{JT}} = -g^2/2K$ (in which K is the elastic energy and g is the electron–lattice coupling constant). The Fourier-transformed Hamiltonian of Eq.(2) is written as

$$H_{\text{eff}} = -\sum_k E_k c_k^+ c_k - E_0\sum_k n_{lk} + J\sum_{\langle ij\rangle}\cos\theta_{ij}, \quad (3)$$

where $E_0 = \varepsilon_{\text{JT}} + Un_b$, $E_k = \varepsilon_k + Un_l$, $\varepsilon_k = -2t\left(\cos k_x a + \cos k_y a + \cos k_z a\right)$.

In the event of a large JT distortion resulting in band splitting (~ 1 eV) there is the possibility that the lower e_g orbital (i.e. the one described by the operators c_k) hybridizes with the localized t_{2g} orbitals (i.e., the operators l_k) which will modify the magnetic ordering of the t_{2g} electrons. Thus the hybridization of the localized electrons with the conduction electrons is considered, and the Hamiltonian H_v which represents this hybridization effect is given by

$$H_v = V\sum_k\left(c_k^+ l_k + l_k^+ c_k\right). \quad (4)$$

Electron–phonon interaction results from the volume dependence of the bare hybridization parameter V. Due to factors like pressure, temperature, doping and other interactions, the hybridization parameter becomes a function of volume or volume strain ε_i at site. We expand the hybridization parameter:

$$V(\varepsilon_i) = V(i) + \varepsilon_i\frac{\partial V_i}{\partial\varepsilon_i}. \quad (5)$$

The instantaneous volume strain (ε_i) can be expressed in terms of phonon creation (annihilation) operators $b_q^+(b_q)$ at the site $\boldsymbol{R}_i$ as

$$\varepsilon_i = \left(|q|/\sqrt{2N_0 M\omega_q}\right)\left(b_q + b_{-q}^+\right)\exp\left(\text{i}\boldsymbol{q}\cdot\boldsymbol{R}_i\right), \quad (6)$$

where M, N_0 and ω_q are the ion mass, the number of sites and the phonon energy, respectively.

The electron–phonon interaction term in the site representation can be written as

$$H_{\text{e-p}} = \sum_i\left(c_i^+ l_i + l_i^+ c_i\right)\varepsilon_i\frac{\partial V_i}{\partial\varepsilon_i}. \quad (7)$$

The Fourier transformed electron–phonon interaction Hamiltonian is

$$H_{\text{e-p}} = \sum_i f(q)\left[c_{k+q}^+ l_k + l_{k+q}^+ c_k\right]\left(b_{-q}^+ + b_q\right), \quad (8)$$

where $b_q(b_q^+)$ are annihilation (creation) operators for phonons with wave vector q, and $f(q)$ is the electron–phonon coupling constant. The electron–phonon coupling constant is given by

$$f(q) = \left(|q|/\sqrt{2N_0 M\omega_q}\right)\frac{\partial V_i}{\partial\varepsilon_i}. \quad (9)$$

The free phonon Hamiltonion with phonon energy ω_q is written as

$$H_p = \sum_q \omega_q b_q^+ b_q. \quad (10)$$

The total Hamiltonian of the system then becomes

$$H = H_{\text{eff}} + H_v + H_{\text{e-p}} + H_p. \quad (11)$$

3. Calculation of the phonon Green function

The phonon self-energy is evaluated by the double-time Green function technique of Zubarev[13] using the method of the equation of motion. The

phonon Green function is defined as

$$D_{qq'}(t-t') = \ll A_q(t); A_{q'}(t') \gg = -\mathrm{i}\Theta(t-t')\langle[A_q(t), A_{q'}(t')]\rangle, \tag{12}$$

where

$$A_q = b_q + b_{-q}^{+} \tag{13}$$

is the qth Fourier component of the displacement. To derive the phonon Green function $D_{q,q'}(t-t')$, we use the equation of motion for phonon operators,

$$\mathrm{i}\frac{\mathrm{d}A_q(t)}{\mathrm{d}t} = [A_q(t), H] = A_q(t)H - HA_q(t). \tag{14}$$

The equation of motion[14] for the Fourier transformed phonon Green function $D_{q,q'}(\omega)$ is evaluated for the system using the total Hamiltonian H given in Eq.(11). The Green function is expressed as

$$D_{q,q'} = \delta_{q,q'}D_q^0(\omega) + 4f^2(-q)D_q^0(\omega)\chi_{q,q'}(\omega)D_q^0(\omega), \tag{15}$$

where

$$D_q^0(\omega) = 2\omega_q\left[\omega^2 - \omega_q^2\right]^{-1}. \tag{16}$$

is the free phonon propagator, and $\chi_{q,q'}(\omega)$ is the electron response function. Applying the Dyson approximation to Eq.(15), we can write the phonon Green function as

$$D_{q,q}(\omega) = 2\omega_q\left[\omega^2 - \omega_q^2 - \sum_q(\omega)\right]^{-1}, \tag{17}$$

where the phonon self-energy

$$\sum_q(\omega) = 4f^2(-q)\omega_q\chi_{q,q}(\omega) \tag{18}$$

depends on the electron response functions $\chi_{q,q}(\omega)$. During the calculation we make some approximations in order to keep the essential physics intact. We use certain decoupling schemes for the higher-order Green functions such that all the physical parameters such as l-level, hybridization term ($\sim V^2$) and phonon coupling term are retained. The limit of zero wave vector ($q \to 0$) and low temperature ($T \to 0$) is considered here in evaluating the response function.

4. Phonon spectral density

The phonon self-energy depends on different model parameters through the electron response function $\chi_{0,0}(\omega)$. In order to compare the theoretical calculations with the experimental results, we need to calculate the spectral density function $S(0,\omega)$, which is a measurable quantity in Raman scattering experiments. The spectral density function is defined through the equation

$$S(0,\omega) = -2\mathrm{Im}D_{qq}(\omega + \mathrm{i}\eta)_{q=0}. \tag{19}$$

The $S(0,\omega)$ is calculated by attributing a finite width (η) to the phonon frequency ($\omega^2 \to \omega^2 + 2\mathrm{i}\omega\eta$). The spectral density function is written as

$$S(0,\omega) = \frac{2\omega_0 B_1(\omega)}{A_1^2(\omega) + B_1^2(\omega)}. \tag{20}$$

Where

$$A_1(\omega) = \omega^2 - \omega_0^2 - \eta^2 + \omega_0^2 A_2(\omega),$$
$$B_1(\omega) = 2\eta\omega + \omega_0^2 B_2(\omega). \tag{21}$$

A_2 and B_2 are written as

$$A_2(\omega) = 8g\int\frac{\mathrm{d}\varepsilon_k A_3}{\omega_1 - \omega_2}H(E_k)[f(\omega_1) - f(\omega_2)],$$
$$B_2(\omega) = 8g\int\frac{\mathrm{d}\varepsilon_k B_3}{\omega_1 - \omega_2}H(E_k)[f(\omega_1) - f(\omega_2)]. \tag{22}$$

Where

$$A_3 = \frac{A_4}{A_4^2 + B_4^2}, \qquad B_3 = \frac{B_4}{A_4^2 + B_4^2},$$
$$A_4 = \omega^2 - (E_k - E_0)^2 - 4V^2 - \eta^2, \qquad B_4 = 2\omega\eta,$$
$$H(E_k) = 2(E_k - E_0)^2,$$
$$\omega_{1,2} = \frac{\varepsilon_k + \varepsilon_{\mathrm{JT}} + 0.5U \pm \sqrt{[\varepsilon_k - \varepsilon_{\mathrm{JT}} + U(2n_l - 0.5)]^2 + 4V^2}}{2}. \tag{23}$$

To understand the influence of the physical quantities on the phonon spectral density function, we scale the parameters by the Debye temperature ω_{D} (= 430K). The dimensionless parameters are the position of the bare l-level $d = \varepsilon_{\mathrm{JT}}/\omega_{\mathrm{D}}$, the hybridization between the l-electrons and the con-

duction $v = V/\omega_D$, the reduced temperature $t = k_B T/\omega_D$, the energy of the conduction electrons $x = \varepsilon_k/\omega_D$, the phonon coupling to the hybridization between the l-electrons and conduction electrons $g = N(0) f^2(0)/\omega_0$, where $N(0)$ is the density of states of conduction electrons at the Fermi level (ε_F), the Coulomb interaction $u = U/\omega_D$ and the bare phonon frequency ($p = \omega_0/\omega_D$).

5. Results and discussion

Figures 1–3 show the variation of spectral density function $S(0,\omega)$ with reduced frequency $\tilde{\omega} = \omega/\omega_0$ for different values of d, v and g at fixed values of reduced temperature t. We observe that there are three peaks in each of these plots. These three peaks appear at $\tilde{\omega} \sim 0.27$, $\tilde{\omega} \sim 0.64$ and $\tilde{\omega} \sim 1.18$ corresponding to P_1, P_2 and P_3 phonon peak respectively. To compare with the experimental results, we estimate the wave number from the relation $hnc = k_B p \omega_D \tilde{\omega}$ (h is Planck's constant, n is the wave number, c is the speed of light). When $\tilde{\omega} \sim 0.27$, $\tilde{\omega} \sim 0.62$ and $\tilde{\omega} \sim 1.18$, the corresponding wave numbers are 105 cm^{-1}, 249 cm^{-1} and 458 cm^{-1} respectively. Granado *et al*[15] found that the Raman peaks of $La_{0.5}Ca_{0.5}MnO_3$ appear at 110(ω_1), 261(ω_2) and 448 cm^{-1}(ω_3), which are very similar to our results. It also confirms the experiments of Antonakos *et al*,[16] whose peaks appear at 80(ω_1), 230(ω_2) and 400–480 cm^{-1}(ω_3). It is generally accepted that in the ω_1 region the band at 110 cm^{-1} of

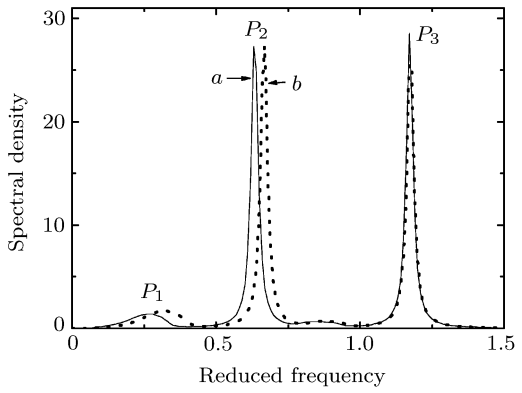


Fig.1. Plot of spectral density function $S(0,\omega)$ vs reduced frequency $\tilde{\omega} = \omega/\omega_0$ at fixed values of $v = -0.05$, $g = 0.055$, $t = 0.09$, $u = 0.49$, $p = 1.3$: (curve a) $d = -1.0$; (curve b) $d = -0.94$.

A_g symmetry is attributed to the $R(x)$ mode of its selection rules, the ω_2 mode appearing as a strong broad band of A_g symmetry is related to the A_g (2) tilting mode and the ω_3 mode has the B_{2g} symmetry.[15,16]

It can be observed from Fig.1 that the P_1 and P_2 peaks show a red shift, and the P_3 peak does not shift with the increase of $|d|$. We also found that the intensity of the peaks P_1 and P_3 increases with the increase of $|d|$, but the intensity of the P_2 peak does not change. Figure 2 exhibits the influence of hybridization parameter in the $S(0,\omega)$ vs $\tilde{\omega}$ plot. Here we take $v = 0.09$, 0.05 respectively. We found that the three peak positions remain unchanged. In order to distinguish clearly, we made a figure for $v = 0.05$ and inset it into Fig.2. It is observed that the intensity of the peaks P_1 and P_3 increases with the increase of v, but the intensity of the P_2 peak does not change. Figure 3 presents the plot of $S(0,\omega)$ vs $\tilde{\omega}$ for $g = 0.055$ and $g = 0.065$. Since the phonon is coupled to the weak hybridization between conduction electrons

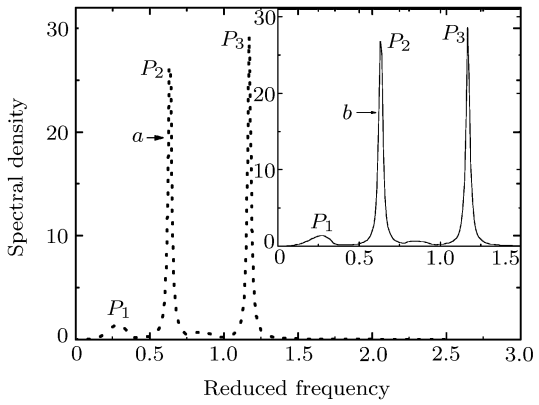


Fig.2. Plot of spectral density function $S(0,\omega)$ vs reduced frequency $\tilde{\omega} = \omega/\omega_0$ at fixed values of $d = -0.94$, $g = 0.055$, $t = 0.09$, $u = 0.49$, $p = 1.3$: (curve a) $v = 0.09$; (curve b) $v = 0.05$.

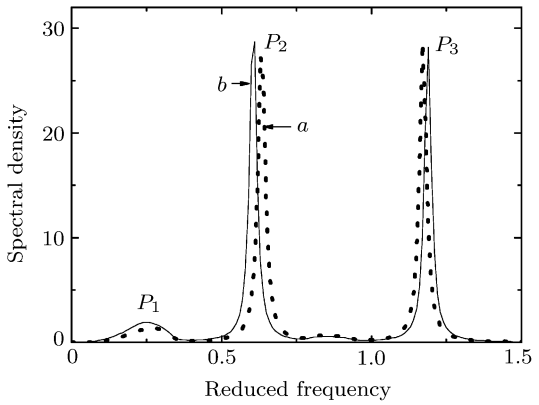


Fig.3. Plot of spectral density function $S(0,\omega)$ vs reduced frequency $\tilde{\omega} = \omega/\omega_0$ at fixed values of $d = -0.94$, $v = 0.05$, $t = 0.09$, $u = 0.49$, $p = 1.3$: (curve a) $g = 0.055$; (curve b) $g = 0.065$.

and l-electrons, the electron–phonon coupling parameter g is small in magnitude. It is observed that the P_1

and P_2 peaks show a red shift and the P_3 peak shows a blue shift with the increase of g. It is also observed that the intensity of the P_1 and P_2 peaks increases with increasing of g while the P_3 peak does not change. It is well known that a longitudinal phonon always accompanies a change of crystal volume and a local change of lattice constant. From deformation potentials of the electron–phonon interaction $\delta\varepsilon_{\rm c} = c_1\Delta(r)$ ($\delta\varepsilon_{\rm c}$ is deformation potentials, c_1 is constant, $\Delta(r)$ is volume change),[17] an increase of g means that electron–phonon coupling increases, which leads to an increase of distortion of the lattice and an appearance of blue shift of the Raman spectrum peaks, which can also be found in Ref.[18].

In our model v is a function of pressure. From the above discussions, we found that all peak positions remain unchanged while their intensities increase with v. In other words, when pressure increases, the intensities of the peaks increase but their positions remain unchanged, which is consistent with the experimental results of Refs.[8, 17]. The parameter d correlates with JT distortions: the increase of d means that JT distortions increase. When JT distortions increase, the Raman spectrum peaks exhibit a shift to higher frequencies, which is noted in Ref.[18].

References

[1] Xiong M, Chen T, Wang G Y, Chen X H, Chen X and Chen C L 2004 *Phys. Rev.* B **70** 094407

[2] Liarokapis E, Leventouri T, Lampakis D, Palles D, Neumeier J J and Goodwin D H 1999 *Phys. Rev.* B **60** 12758

[3] Smolyaninova V N, Biswas Amlan, Zhang X, Kim K H, Kim Bog Gi, Cheong S W and Greene R L 2000 *Phys. Rev.* B **62** R6093

[4] Cao X S, Xiao C T, Gywn Williams and Roy Roshko 2005 *Chin. Phys.* **14** 1051

[5] Tang W H, Li P G, Lei M, Guo Y F, Chen L M, Li L H, Song P Y and Chen C P 2006 *Chin. Phys.* **15** 767

[6] Zhang N, Geng T, Cao H X and Bao J C 2008 *Chin. Phys.* B **17** 317

[7] Kim M, Barath H, Cooper S L, Abbamonte P, Fradkin E, Rübhausen M, Zhang C L and Cheong S W 2008 *Phys. Rev.* B **77** 134411

[8] Iliev M N and Abrashev M V 2001 *J. Raman Spectrosc* **32** 805

[9] Iliev Milko N, Abrashev M V, Popov V N and Hadjiev V G 2003 *Phys. Rev.* B **67** 212301

[10] Zhao J H, Chen B and Wang D L 2008 *Acta. Phys. Sin.* **57** 3077 (in Chinese)

[11] Kugel K I, Rakhmanov A L and Sboychakov A O 2005 *Phys. Rev. Lett.* **95** 267210

[12] Ramakrishnan T V, Krishnamurthy H R, Hassan S R and Pai G V 2004 *Phys. Rev. Lett.* **92** 157203

[13] Zubarev D N 1960 *Sov. Usp.* **3** 320

[14] Elk K 1974 *Phys. Stat. Sol.* (b) **64** 489

[15] Granado E, Moreno N O, Garc´ia A, Sanjurjo J A, Rettori C, Torriani I, Oseroff S B, Neumeier J J, McClellan K J, Cheong S W and Tokura Y 1998 *Phys. Rev.* B **58** 11435

[16] Antonakos A, Liarokapis E, Aydogdu G H and Habermeier H U 2007 *Materials Science and Engineering* B **144** 83

[17] Bardeen J and Shockley W 1950 *Phys. Rev.* **80** 72

[18] Amelitchev V A, Güttler B, Gorbenko O Yu, Kaul A R, Bosak A A and Ganin A Y 2001 *Phys. Rev.* B **63** 104430